Effect of tip geometry on local indentation modulus measurement via atomic force acoustic microscopy technique

D. Passeri, A. Bettucci,[a] M. Germano, M. Rossi, and A. Alippi
Dipartimento di Energetica, Università di Roma "La Sapienza", Via Antonio Scarpa 16, 00161 Roma, Italy

S. Orlanducci and M. L. Terranova
Dipartimento di Scienze e Tecnologie Chimiche, Università di Roma "Tor Vergata" and Micro and Nano-structured Systems Laboratory (MINASlab), Via della Ricerca Scientifica, 00133 Roma, Italy

M. Ciavarella
CEMEC-PoliBA -Centre of Excellence in Computational Mechanics, Politecnico di Bari, Viale Japigia 182, 70125 Bari, Italy

(Received 13 April 2005; accepted 7 August 2005; published online 7 September 2005)

Atomic force acoustic microscopy (AFAM) is a dynamical AFM-based technique very promising for nondestructive analysis of local elastic properties of materials. AFAM technique represents a powerful investigation tool in order to retrieve quantitative evaluations of the mechanical parameters, even at nanoscale. The quantitative determination of elastic properties by AFAM technique is strongly influenced by a number of experimental parameters that, at present, are not fully under control. One of such issues is that the quantitative evaluation require the knowledge of the tip geometry effectively contacting the surface during the measurements. We present and discuss an experimental approach able to determine, at first, tip geometry from contact stiffness measurements and, on the basis of the achieved information, to measure sample indentation modulus. The reliability and the accuracy of the technique has been successfully tested on samples (Si, GaAs, and InP) with very well known structural and morphological properties and with indentation modulus widely reported in literature. © *2005 American Institute of Physics.*
[DOI: 10.1063/1.2044607]

I. INTRODUCTION

Decreasing of length scale in the realization of integrated devices, such as microelectromechanical systems (MEMSs),[1] requires the development of instruments and techniques capable of characterizing mechanical, electrical, and optical properties of materials[2] as well as of devices[3] with submicrometrical spatial resolution. Scanning probe microscopy (SPM)-based analysis and spectroscopy represents a powerful investigation tool, allowing one to probe sample surfaces at nanometrical scale and to acquire wide information representing not only its morphological characteristics but even its local mechanical properties. A number of different techniques have been developed in order to retrieve quantitative evaluations of the mechanical parameters. Based on atomic force microscopy (AFM),[4] ultrasonic force microscopy[5–7] (UFM), and atomic force acoustic microscopy[8–11](AFAM) are emerging techniques for the investigation of elastic properties of materials, being used in the past to image and measure local mechanical properties of different hard samples, such as piezoelectric ceramics,[12] crystalline materials,[6] nanocrystalline ferrites,[13] diamondlike carbon coatings,[14] and niobium films.[15]

AFAM is a dynamical AFM technique where the measuring procedure is based on the detection of the mechanical resonance frequencies of a vibrating cantilever. Elastic parameters are deduced from resonance frequency shifts in contact resonance spectroscopy (CRS) measurements in the two cases of a free cantilever vibrating in air and a cantilever vibrating in contact with the sample surface.[11,14] AFAM is a very promising technique whose employment has been successfully demonstrated on samples with a wide range of Young modulus values. Nevertheless, the quantitative determination of elastic properties with the AFAM technique is influenced by a number of experimental parameters, such as humidity,[16] microscope tip radius changes due to abrasion,[14] and geometry of the tip. In particular, the evaluation from resonance frequencies of the Young modulus for isotropic materials, or of the indentation modulus for anisotropic materials, requires the knowledge of the tip shape contacting the surface, as in indentation tests.[17–19] More specifically, supposing that the sample surface is plain and that one has no further information about the tip geometry, a range of possible elastic modulus values can be estimated by considering the two limiting cases of spherical (Hertzian contact) and flat tips.[15] Moreover, depending on the normal static load applied to the sample by AFM cantilever, the lack of information about the geometry of the tip can lead to a substantially erroneous interpretation of the experimental data.

In previous articles,[6,12] it was suggested to deduce information on AFM tip geometry by contact stiffness versus applied normal static load curves. In this work, we examine closely such idea, presenting some experimental results obtained performing AFAM measurements on crystalline

[a]Electronic mail: andrea.bettucci@uniroma1.it

samples whose elastic parameters are given in literature. From contact stiffness versus normal static load plots, static load ranges can be determined in which the tip exhibits a behavior clearly ascribable to Hertzian or a flat punch contact, as well as ranges in which its behavior cannot be described by a simple model. In the first case, measured contact stiffness values are used to evaluate the sample local indentation modulus. In the second case, since contact stiffness values are not simply related to surface elastic parameters, they are neglected in order to avoid erroneous interpretation of the experimental data.

Moreover, in the AFAM technique relatively high normal static loads are required in order to neglect the effects of adhesion.[20–22] In order to satisfy such issue, a cantilever with a high spring constant should be chosen. Nevertheless, the spring constant of the available commercial cantilevers can be so high that applied normal stresses can be comparable to the yield strength or to the hardness of employed materials. In this case, damages to the tip apex can occur, leading to a modification in the tip geometrical parameters while performing AFAM measurements. For such reasons, in the present work, the description of our experimental results is supported by considerations on the effects of high static loads applied on the tip.

In the following, first the AFAM technique and experimental procedure are described then the samples on which measurements were performed. In order to verify the reliability and the accuracy of the technique, samples were chosen for which physical data are available. Finally, some experimental results are presented, wherefrom information is deduced on tip geometry and indentation modulus is evaluated and compared with the values reported in literature.

II. EXPERIMENT

A. AFAM technique

In order to deduce the analytical relationships between contact resonance spectra and local indentation modulus, the AFM cantilever can be modeled as a beam, with a uniform rectangular cross section, with length L, width w, and thickness t, clamped at one end.[8] The general case of a nonuniform cross section requires a finite-element approach[15] and it will not be considered in the following description. In the first step of the experimental procedure, the cantilever is free to vibrate, out of contact from the sample surface (clamped-free configuration). The flexural vibration modes of the clamped-free cantilever solve the characteristic equation[8,23]

$$\cos(k_n L)\cosh(k_n L) + 1 = 0, \tag{1}$$

and the wave numbers k_n's are related to the resonance frequencies through the equation[8]

$$f_n = \frac{(k_n L)^2}{c_c^{\,2}}. \tag{2}$$

The characteristic constant of the cantilever c_c can be deduced experimentally from the set of f_n frequencies, since the values of $k_n L$ that solve Eq. (1) are well known.[8,23]

In the second step of the experimental procedure, the cantilever is brought into contact with the sample surface and the tip-sample interaction modifies the boundary conditions for the vibrating cantilever. Though strongly nonlinear,[10,24] for small vibration amplitudes, the interaction can be modeled by a linear spring with elastic constant k^*, representing the contact stiffness, as sketched in Fig. 1, where the tip is at a distance L_1 from the cantilever clamped end.[10] From the characteristic equation of the system shown in Fig. 1, the following expression for k^* can be obtained:[8,11]

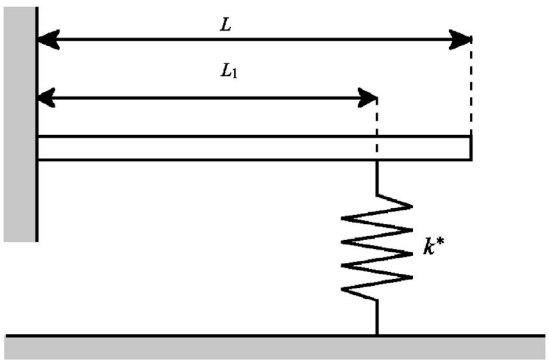

FIG. 1. Equivalent linear model for AFM cantilever contacting sample surface. The tip is supposed to be placed at distance L_1 from the cantilever clamped end, while L is the cantilever length. The tip-sample contact stiffness is described by a linear spring with constant k^*.

$$\begin{aligned} k^* = {} & \tfrac{2}{3}k_c(k_n L r)^3(1+\cos k_n L \cosh k_n L)/ \\ & \{-(\cosh k_n L r \sin k_n L r - \sinh k_n L r \cos k_n L r) \\ & \times[1+\cos(1-r)k_n L \cosh(1-r)k_n L] + [\cosh(1 \\ & - r)k_n L \sin(1-r)k_n L - \sinh(1-r)k_n L \cos(1-r)k_n L] \\ & \times(1-\cos k_n L r \cosh k_n L r)\}, \end{aligned} \tag{3}$$

where r is the ratio L_1/L and k_c is the spring constant of the cantilever. The value of k^* can be calculated from the measured contact resonance frequencies. That result shifted to higher values with respect to free resonance frequencies,[10] as it can be seen by replacing in Eq. (3) the expression for $k_n L$ obtained from Eq. (2). The value of r, used in Eq. (3) as a free fitting parameter, can be evaluated by matching the expressions of k^* obtained at two different modes.[13] Moreover, the values of k^* obtained from different pairs of resonance frequencies can be used to estimate the absolute error of the method.[11]

The value of k^*, in case that the contact area can be considered as a circle with radius a, is related to the sample indentation modulus by the equations[17,25]

$$E^* = \frac{k^*}{2a} \tag{4}$$

and

$$\frac{1}{E^*} = \frac{1}{M_s} + \frac{1}{M_t}, \tag{5}$$

where E^* is the reduced Young modulus and M_s and M_t are the indentation moduli of the sample and tip, respectively. Eq. (4) is, generally, valid for an axisymmetric tip, i.e., for a tip that can be described as a solid of revolution around a symmetry axis normal to the sample surface.[17] For isotropic

materials and axisymmetric geometries, the indentation modulus M is related to the Young modulus E and to the Poisson ratio ν by the equation

$$M = \frac{E}{1-\nu^2}, \tag{6}$$

which is independent of the tip shape. In the general case of anisotropic materials, M has to be numerically evaluated from the elements c_{ij} of the stiffness tensor.[26–28] The expression of a in Eq. (4) depends on the geometry of the tip. For a spherical tip contacting a flat surface, i.e., the Hertzian contact, it is given by the expression[25]

$$a = \sqrt[3]{\frac{3F_N R}{4E^*}}, \tag{7}$$

F_N being the normal static load applied to the sample surface and R the tip radius. The value of F_N, if adhesion forces are negligible,[20–22] can be calculated as $k_c d$, where d is the deflection of the cantilever. For Hertzian contact, the relation between k^* and F_N can be obtained combining Eq. (4) and (7),

$$k^* = \sqrt[3]{6E^{*2}RF_N}. \tag{8}$$

For a flat punch contacting a flat surface, a and k^* are constant and independent from the applied normal static load.

In both the cases of spherical and flat tips, the value of the contact radius a is unknown and has to be evaluated by performing AFAM measurement on a reference sample. The reduced Young modulus of the sample under test is given by[9]

$$E_s^* = E_{\mathrm{ref}}^* \left(\frac{k_s^*}{k_{\mathrm{ref}}^*}\right)^n = E_{\mathrm{ref}}^* \left(\frac{k_s^*/k_c}{k_{\mathrm{ref}}^*/k_c}\right)^n, \tag{9}$$

$E_s^*, k_s^*, E_{\mathrm{ref}}^*$ and k_{ref}^* being the reduced Young moduli and the calculated contact stiffnesses of the unknown and reference samples, respectively. The value of n depends on the geometry of the tip: for a flat punch it is $n=1$ while for a spherical tip it is $n=3/2$, if measurements on the reference sample and on the sample under test are performed at the same value of F_N. By using Eq. (8), in the case of a spherical tip, Eq. (9) can be written in the form

$$E_s^* = E_{\mathrm{ref}}^* \sqrt{\frac{(k_s^*)^3}{F_{N,s}} \frac{F_{N,\mathrm{ref}}}{(k_{\mathrm{ref}}^*)^3}} = E_{\mathrm{ref}}^* \sqrt{\frac{(k_s^*/k_c)^3}{F_{N,s}} \frac{F_{N,\mathrm{ref}}}{(k_{\mathrm{ref}}^*/k_c)^3}}, \tag{10}$$

where the term under the square root is the ratio between the slopes of the $(k^*)^3$ versus F_N curves for the sample and the reference, respectively.

B. Experimental setup and sample description

The AFAM apparatus used in the present work is a commercial AFM (Smena, NT-MDT, Russia) equipped with a piezoelectric transducer, that can excite longitudinal oscillations at ultrasonic frequencies in the sample under investigation. Measurements were performed using four commercial rectangular (100) silicon cantilevers (Mikromasch, nominal dimensions: $L=230\pm5$ μm, $w=40\pm3$ μm, and $t=7\pm0.5$ μm) with spring constant k_c estimated by the producer in the range of 25–60 N/m. A more accurate evaluation of the spring constant was obtained by measuring cantilevers first free resonance frequency and its quality factor in air, neglecting the 30-nm-thick reflective Al coating:[29,30] due to the low value of aluminum mass density, this may introduce an experimental error of about ±1% in the calculated values of k_c. In order to reduce the experimental error in determining the cantilever spring constant, which affects the evaluation of both tip-sample contact stiffness and applied static normal load, geometrical dimensions and shapes of the cantilevers were deduced from scanning electron microscopy (SEM) observation. In particular, cantilever cross sections were found to be trapezoidal, while rectangular sections with average widths were supposed in evaluating k_c with the method of Sader *et al.*[29,30] Consequently, the total uncertainty in calculating the k_c values for the four cantilevers can be estimated to about 11%. It is worthwhile to note that such uncertainty does not affect the calculated values of E^* [see Eqs. (9) and (10)] but only the determination of the normal static load applied by the cantilevers on the samples.

AFAM measurements were performed on Si, GaAs, and InP crystalline samples, all oriented along the (100) crystallographic direction, which are cases where the stiffness tensors are all well known.[31–34] In order to avoid abrasion of the tip and the consequent modification of its radius, sample surfaces were not imaged during the experiment. When necessary, topographic images of the three samples were acquired apart from the AFAM measurements. Furthermore, a possible source of systematic error was removed by repeating the measurements on the samples exchanging their temporal order. (100) Si was used as the reference sample, as explained in Sec. II A in order to retrieve information on the unknown radius of the AFM tip. Each sample was approached by the AFM tip and contact resonance spectra were collected for increasing values of the static normal load in different ranges, as reported in Table I.

III. RESULTS AND DISCUSSION

In CRS measurement, the first two contact resonance frequencies, namely, f_1 and f_2, are experimentally determined at increasing values of the applied normal static load F_N, thus calculating the corresponding contact stiffness k^* values. Figure 2 reports a typical measured contact stiffness versus applied static normal load, obtained using cantilever *A* on the Si, GaAs, and InP samples, respectively. It is worthwhile to observe that for values of F_N increasing from 1 to 3 μN, the dependence of k^* on the static normal load cannot be ascribed neither to a spherical or a flat AFM tip geometry, since measured k^* values result neither independent from F_N, as for flat punchlike tip, nor proportional to $(F_N)^{1/3}$, as for Hertzian contact. Therefore, in this range, the measured values of k^* do not allow to correctly estimate sample indentation moduli. By increasing the normal static load beyond 3 μN, the saturation effect of the contact resonance frequency shift was observed, leading to limit the k^* values for the three samples. Similar plateau regions have been obtained for all the tips. It should be explicitly pointed out that, in the whole range of applied normal load, calculated contact stiffness values are from 80 to 130 times larger than the cantilever spring constant k_c, allowing one to neglect friction

TABLE I. Measured values of the indentation moduli M for the GaAs and InP samples in the (100) crystallographic orientation, obtained with the four cantilevers. For comparison, the numerically calculated indentation modulis of GaAs and InP are also reported. The indentation modulus of Si (100) has been assumed to be equal to $M_{Si(100)}=164.8$ GPa. For each M value, the stress τ under the tip involved in the measurement is estimated. For each cantilever, the calculated spring constant k_c is reported.

		GaAs		InP	
Cantilever	k_c(N/m)	M (GPa)	τ (GPa)	M (GPa)	τ (GPa)
A	33	117±2	2–3.6	88±1	2–3.1
B	27	112±2	3.2–6.5	92±2	0.9–2.4
C	38	124±5	0.3–1.3	96±9	0.5–2.4
D	43	125±12	0.9–2.4	96±14	0.9–2.4
Calculated		117.4		92.1	

effects in the model previously described.[35] The independence of k^* from F_N is not due to the tip-sample pinned end condition.[8] In this case, in fact, contact resonance frequencies can be easily evaluated numerically solving Eq. (3) for $k^* \to \infty$ [$r=0.94\pm0.01$ is experimentally determined comparing the expressions of k^* obtained for f_1 and f_2 (Ref. 13)] resulting in calculated limit frequencies significantly higher than the measured ones.

The radius a of the contact area involved in each measurement was evaluated from Eq. (4) in order to estimate the range of the pressure exerted by the tip on the sample and to verify the possibility of plastic deformation in the silicon tip. Stress value ranges involved in each measurement are reported in Table I. It should be noted that saturation effect in the experimental k^* value is observed even for stress values significantly lower than the yield strength value of 7 GPa reported for Si in literature at room temperature.[36] Moreover, no differences in the k^* versus F_N experimental curves have been observed while increasing the pressure exerted by the tip up to values comparable with silicon yield strength, as for cantilever *B*. Consequently, the observed saturation in the k^* versus F_N curves cannot be attributed to effects of plastic deformation of the AFM tip, even if such deformation cannot be excluded in some of the reported measurements.

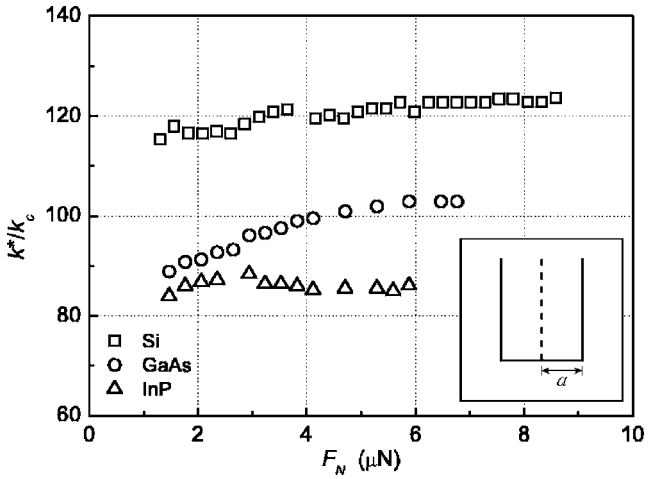

FIG. 2. Measured contact stiffness values k^*/k_c as a function of applied normal static load F_N, for Si, GaAs, and InP samples, obtained from the first and second contact resonance frequencies of cantilever *A*. In the inset, the geometrical model is sketched, modeling the tip as a circular flat punch with contact radius $a=25$ nm.

The plateau in the k^* curves reported in Fig. 2 can be rationalized by supposing that for normal static load values higher than 3 μN the cantilever tip acts as a flat punch indenting a plain surface. From the c_{ij} elements of the stiffness tensor reported in literature,[31–34] indentation moduli in the (100) crystallographic orientation were numerically evaluated for Si, GaAs, and InP, through the method of the Green functions, as widely described in Ref. 28, leading to the values $M_{Si(100)}=164.8$ GPa, $M_{GaAs(100)}=117.4$ GPa, and $M_{InP(100)}=92.1$ GPa. As described above, the calculated Si (100) indentation modulus was used as a reference value, and GaAs and InP indentation moduli have been calculated from the experimental saturation k^* values, using Eqs. (5) and (9), where $n=1$ is assumed for a tip modeled as a flat punch. The measured values of indentation moduli obtained with the four cantilevers, resumed in Table I, are in good agreement with the calculated ones. The experimental error has been calculated on the basis of multiple measurements on both reference (Si) and investigated samples (GaAs and InP). It should be explicitly pointed out that, in the present case, there is no need to calculate E by averaging the values obtained in considering $n=1$ and $n=3/2$ in Eq. (9), since the geometry of the cantilever tip is actually known from k^* versus F_N curves. Moreover, substituting data concerning Si sample in Eqs. (4) and (5), the radius a of the flat contact can be evaluated: for example, for cantilever A, $a=25$ nm, a value that is coherent with the manufacturer's data considering abrasion effect due to usage of the tip.

In order to confirm the supposed flatness of the apex, SEM analysis has been performed on the used tips. In Figs. 3(a) and 3(b), top and side views are reported for a brand new tip. In Figs. 3(c) and 3(d), top and side views are reported for the tip of cantilever *B* (similar shapes of the tip apex have been found in cantilevers A, C, and D) as it appears after some AFAM measurement sessions. In the two latter images, a wide flat region is clearly observed on the tip, thus confirming the interpretation of the independence of measured k^* from F_N as the effect of the flat profile of the AFM tip.

It should be explicitly observed from data reported in Table I that the stress values involved in some of the reported

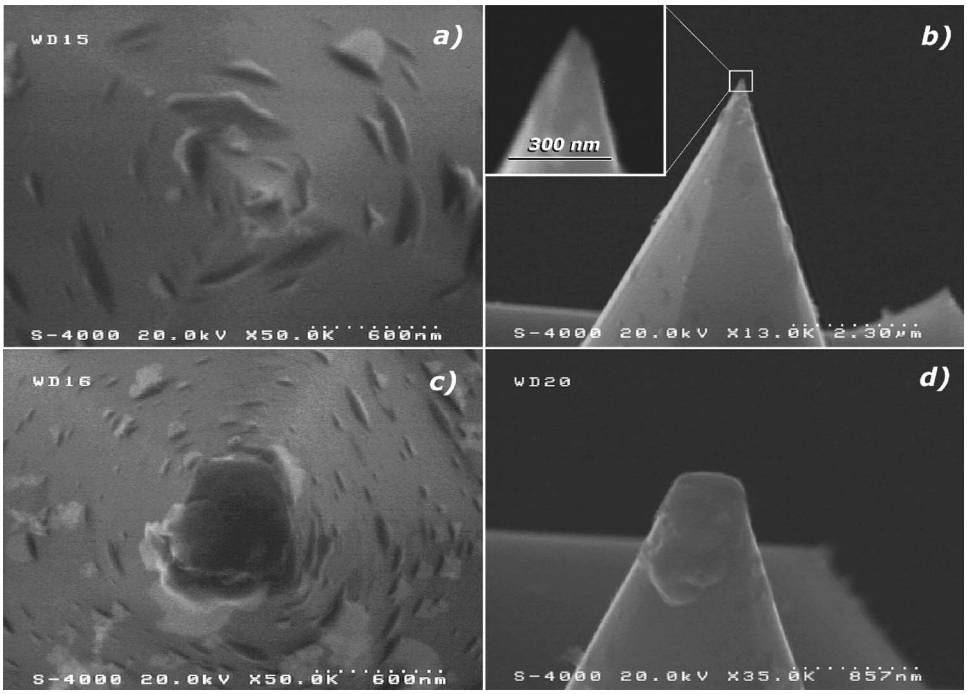

FIG. 3. SEM images of two AFM tips: top (a) and side (b) views of a brand new tip; top (c) and side (d) views of the tip of cantilever *B* after some AFAM measurement sessions.

measurements are comparable to the hardness of the GaAs and InP (100) crystalline samples.[37] Thus, plastic deformations and formation of subsurface cracks may have occurred. Nevertheless, no differences in the k^* versus F_N curves and in the evaluated indentation modulus values can be observed, within the experimental error, for low and high applied static load measurements. Such results suggest that the possible plastic deformations that occurred in the GaAs and InP samples do not significantly modify their measured mechanical properties, in analogy with what was stated in Ref. 37.

Contact stiffness versus normal static load, for each cantilever used in our measurements, shows a behavior similar to the one reported in Fig. 2, suggesting that in all the cantilevers the apex acts as a flat punch, rather than a spherical indenter. Such a result is quite surprising, since a brand new tip is expected to have a spherical apex. An explanation for the commonly found flat punch behavior of AFM tips can be argued observing two subsequent contact stiffness curves, as in Fig. 4. In Fig. 4(a), the measured values of $(k^*)^3$ as a function of F_N are reported. Data have been obtained by evaluating contact resonance frequencies f_1 and f_2 using cantilever *B* for the Si reference sample. Two ranges of normal load are clearly recognizable, in which the AFM tip shows two different behaviors. For applied static normal load values from 2 to 4 μN, $(k^*)^3$ is proportional to F_N, i.e., tip-sample contact can be described by Hertzian theory. Consequently, the tip can be modeled as a sphere, with radius R obtained from Eq. (8). Substituting the value of E^* calculated by Eq. (5), and evaluating the ratio between $(k^*)^3$ and F_N from the slope of the fitting curve in Fig. 4(a), tip radius $R = 16$ nm is obtained, which is coherent with the data sheet of the cantilever.

For applied static normal load F_N values ranging from 500 nN to 1 μN, the measured value of k^* is independent from F_N. Such a behavior is due to the flat profile of the tip and not to adhesion and capillary forces. Neglecting adhe-

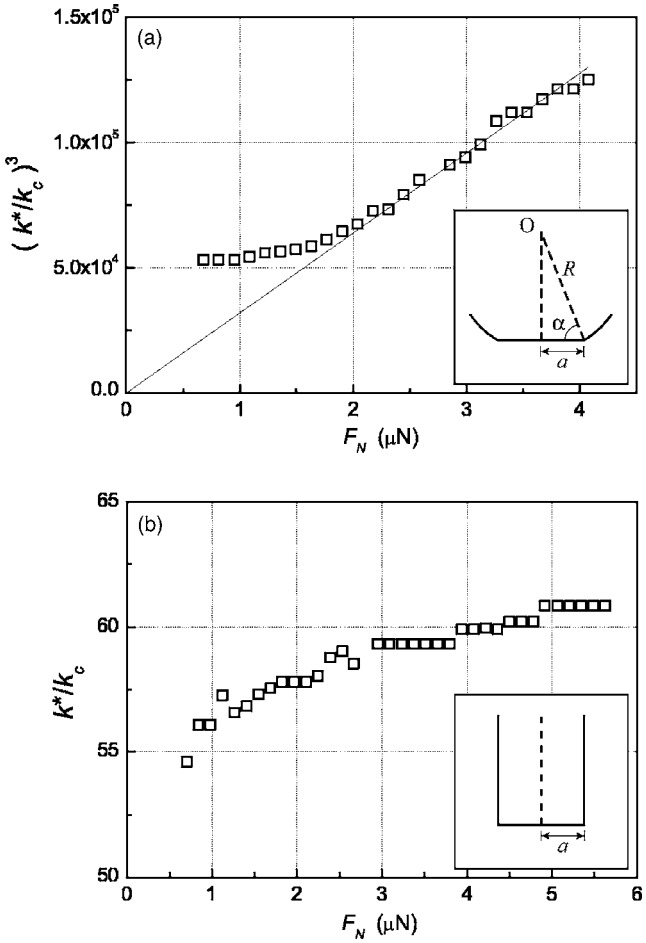

FIG. 4. (a) Measured $(k^*/k_c)^3$ values as a function of applied normal static load F_N for the reference Si sample, obtained from the first and second contact resonance frequencies of cantilever *B*, before damage. In the inset, the geometrical model of the tip is sketched, with calculated parameters $R = 16$ nm, $a = 6$ nm, and $\alpha = 68°$. (b) Measured k^*/k_c values as a function of the applied normal static load F_N for the reference Si sample, obtained from the first and the second contact resonance frequencies of cantilever *B*, after damage. In the inset, the geometrical model for the tip is sketched, modeling the tip as a circular flat punch with contact radius $a = 10$ nm.

sion forces, which is reasonable for AFAM measurement performed in air,[21] capillary forces in the case of a spherical tip contacting a flat surface can be evaluated in tens of nanonewtons, which is negligible with respect to the minimum applied static load.[21,22]

The independence of k^* from F_N can be explained supposing that, for applied static loads lower than 1 μN, the AFM tip behaves as a flat indenter of radius $a=6$ nm, evaluated from Eq. (4). Tip geometry can be modeled as sketched in the inset of Fig. 4(a). By means of simple trigonometric relations, the angle α can be evaluated in 68°. As previously discussed, also in this case friction effects can be neglected since, in the whole range of applied normal load F_N, k^* values are from 39 to 50 times larger than the cantilever spring constant k_c.[35] Repeating the measurement on the GaAs, and InP samples, similar behavior of $(k^*)^3$ versus F_N curves was expected. In particular, for the three samples, the slopes in the region described by Hertzian contact theory were expected to be related one to the other according to Eq. (10), while the k^* values in the region described by a flat punch model were expected to be related according to Eq. (9) with $n=1$. Instead, repeating measurement on the Si, GaAs, and InP samples, using the same cantilever *B*, in the same range of applied normal static load, k^* versus F_N curves show a different behavior, similar to the ones reported in Fig. 2. A typical experimental curve obtained for the same Si reference sample is shown in Fig. 4(b). Such a behavior of k^* versus F_N curves was found to be highly reproducible and similar for the three samples, except for the different k^* values corresponding to different plateaus. It should be considered that, during the measurements whose data are reported in Fig. 4(a), the pressure exerted by the tip on the sample increased up to 18 GPa, which is higher than the Si hardness values of 8–13 GPa reported in literature.[36,38,39] Consequently, a damage in the apex may occur, modifying the geometry of the tip. Such hypothesis is confirmed by SEM analysis of the tip of cantilever *B* after the damage, reported in Figs. 3(c) and 3(d). Experimental curves and SEM analysis suggest that, after the damage, the AFM tip can be modeled as a flat punch indenting a plane, as discussed above, and can be used to retrieve correct measurement of the sample indentation modulus. Experimental data retrieved by cantilever *B* after the damage are reported in Table I. It is possible to suppose that, for the cantilevers used in this work, the small curvature radius of a brand new tip and the high normal static loads involved, due to the high cantilever spring constant, lead to stress values under the apex comparable to the (100) Si hardness values. Damages in the apex geometry may occur, increasing its curvature radius. As a result, the contact between the damaged tip and the sample surface is described by a flat punch better than by a spherical indenter.

ACKNOWLEDGMENTS

This research work has been partially supported by the Italian National Program FISR "Development of technologies and modeling for the synthesis of nanophases and nanostructured materials". The authors gratefully acknowledge S. Berezina-Slabeyciusova for interesting discussions and useful suggestions concerning experimental ultrasonic AFM techniques, J. J. Vlassak for his help in the numerical evaluation of the indentation modulus, and G. Zollo for providing the GaAs and InP samples.

[1] L. S. Fan, Y. C. Tai, and R. S. Muller, IEEE Trans. Electron Devices **35**, 724 (1988).
[2] See, for example, M. Mehregany, and C. A. Zorman, Thin Solid Films **355**, 518 (1999); C. R. Stoldt, M. C. Fritz, C. Carraro, and R. Maboudian, Appl. Phys. Lett. **79**, 347 (2001); H. D. Espinosa, B. Peng, B. C. Prorok, N. Moldovan, O. Auciello, J. A. Carlisle, D. M. Gruen, and D. C. Mancini, J. Appl. Phys. **94**, 6076 (2003); M. P. Tsang, C. W. Ong, N. Chong, C. L. Choy, P. K. Lim, and W. W. Hung, J. Vac. Sci. Technol. A **19**, 2542 (2001).
[3] H. Liu, and B. Bhushan, J. Vac. Sci. Technol. A **22**, 1388 (2004).
[4] G. Binnig, C. F. Quate, and C. Gerber, Phys. Rev. Lett. **56**, 930 (1986).
[5] O. Kolosov, and K. Yamanaka, Jpn. J. Appl. Phys., Part 2 **32**, L1095 (1993).
[6] F. Dinelli, S. K. Biswas, G. A. D. Briggs, and O. Kolosov, Phys. Rev. B **61**, 13995 (2000).
[7] L. Muthuswami, and R. E. Geer, Appl. Phys. Lett. **84**, 5082 (2004).
[8] U. Rabe, J. Janser, and W. Arnold, Rev. Sci. Instrum. **67**, 3281 (1996).
[9] U. Rabe, S. Amelio, M. Kopycinska, S. Hirsekorn, M. Kempf, M. Göken, and W. Arnold, Surf. Interface Anal. **33**, 65 (2002).
[10] U. Rabe, E. Kester, and W. Arnold, Surf. Interface Anal. **27**, 386 (1999).
[11] U. Rabe, S. Amelio, E. Kester, V. Scherer, S. Hirsekorn, and W. Arnold, Ultrasonics **38**, 430 (2000).
[12] U. Rabe, M. Kopycinska, S. Hirsekorn, J. Muñoz Saldaña, G. A. Schneider, and W. Arnold, J. Phys. D **35**, 2621 (2002).
[13] E. Kester, U. Rabe, L. Presmanes, Ph. Tailhades, and W. Arnold, J. Phys. Chem. Solids **61**, 1275 (2000).
[14] S. Amelio, A. V. Goldade, U. Rabe, V. Scherer, B. Bhushan, and W. Arnold, Thin Solid Films **392**, 75 (2001).
[15] D. C. Hurley, K. Shen, N. M. Jennett, and J. A. Turner, J. Appl. Phys. **94**, 2347 (2003).
[16] D. C. Hurley, and J. A. Turner, J. Appl. Phys. **95**, 2403 (2004).
[17] G. M. Pharr, W. C. Oliver, and F. R. Brotzen, J. Mater. Res. **7**, 613 (1992).
[18] N. A. Burnham, and R. J. Colton, J. Vac. Sci. Technol. A **7**, 2906 (1989).
[19] A. L. Weisenhorn, M. Khorsandi, S. Kasas, V. Gotzos, and H. J. Butt, Nanotechnology **4**, 106 (1993).
[20] N. A. Burnham, D. D. Dominguez, R. L. Mowery, and R. J. Colton, Phys. Rev. Lett. **64**, 1931 (1990).
[21] V. Agache, B. Legrand, D. Collard, and L. Buchaillot, Appl. Phys. Lett. **81**, 2623 (2002).
[22] J. N. Israelachvili, *Intermolecular and Surface Forces* (Academic, London, 1985).
[23] D. Sarid, *Scanning Force Microscopy* (Oxford University Press, New York, 1994).
[24] K. Yamanaka, A. Noguchi, T. Tsuji, T. Koike, and T. Goto, Surf. Interface Anal. **27**, 600 (1999).
[25] K. L. Johnson, *Contact Mechanics* (Cambridge University Press, Cambridge, 2003).
[26] J. J. Vlassak, and W. D. Nix, Philos. Mag. A **67**, 1045 (1993).
[27] J. J. Vlassak, and W. D. Nix, J. Mech. Phys. Solids **42**, 1223 (1994).
[28] J. J. Vlassak, M. Ciavarella, J. R. Barber, and X. Wang, J. Mech. Phys. Solids **51**, 1701 (2003).
[29] J. E. Sader, J. W. M. Chon, and P. Mulvaney, Rev. Sci. Instrum. **70**, 3967 (1999).
[30] J. E. Sader, I. Larson, P. Mulvaney, and L. R. White, Rev. Sci. Instrum. **67**, 3789 (1995).
[31] J. J. Wortman, and R. A. Evans, J. Appl. Phys. **36**, 153 (1965).
[32] J. S. Blakemore, J. Appl. Phys. **53**, R123 (1982).
[33] W. A. Brantley, J. Appl. Phys. **44**, 534 (1973).
[34] D. N. Nichols, D. S. Rimai, and R. J. Sladek, Solid State Commun. **36**, 667 (1980).
[35] P. E. Mazeran and J. L. Loubet, Tribol. Lett. **3**, 125 (1997).
[36] K. E. Petersen, Proc. IEEE **70**, 420 (1982).
[37] J. E. Bradby, J. S. Williams, J. Wong-Leung, M. V. Swain, and P. Munroe, Appl. Phys. Lett. **78**, 3235 (2001).
[38] B. Bhushan, and X. Li, J. Mater. Res. **12**, 54 (1997).
[39] I. Yonenaga, J. Phys.: Condens. Matter **14**, 12947 (2002).